Cement and Concrete Research 42 (2012) 827–833

Contents lists available at SciVerse ScienceDirect

Cement and Concrete Research

journal homepage: http://ees.elsevier.com/CEMCON/default.asp

Digital fracture surfaces and their roughness analysis: Applications to cement-based materials

Tomáš Ficker [a,*], Dalibor Martišek [b]

[a] Brno University of Technology, Faculty of Civil Engineering, Department of Physics, Veveří 95, 602 00 Brno, Czech Republic
[b] Brno University of Technology, Faculty of Mechanical Engineering, Department of Mathematics, Technická 2, 616 62 Brno, Czech Republic

ARTICLE INFO

Article history:
Received 26 October 2011
Accepted 13 March 2012

Keywords:
Roughness numbers (B)
Fracture surfaces (B)
Confocal microscopy (B)
Cement-based materials (D)
Fourier functions

ABSTRACT

Roughness numbers employed in morphological analyses characterize height irregularities of solid surfaces, which are also utilized in fractographic studies. In principle, roughness numbers are computed as height differences between the measured height profile and the reference level that has to be implemented into the profile. Positioning reference level is not an unambiguous computational operation and the result depends on the type of optimization procedure as well as the functional pattern used. A wrong position or an inconvenient pattern results in wrong roughness numbers, which devalue morphological analyses. The Fourier series has proved to be a reliable functional pattern capable of optimum positioning within the digitalized height profiles. The whole procedure is illustrated with fracture surfaces of hydrated cement pastes, whose fracture surfaces have been a subject of fractography analyses and morphological studies for several past decades.

1. Introduction

There are no doubts that fractographic studies represent fruitful tools for exploring fracture processes in solid materials [1–7]. Fracture surfaces which are a result of crack propagation bear valuable morphological information on that dynamic process. For example, in brittle materials when the speed of a crack exceeds a specific value, interesting surface morphological changes have been observed in the form of conical objects that decorated fracture surfaces of those materials [1–3].

In fractographic analyses the so-called roughness numbers are commonly used along with other surface parameters to quantify irregularities of fracture surfaces [4,5]. Roughness numbers were initially developed for the classification of surface finishing of sliding metallic surfaces used in some machinery parts but the fracture surfaces of very different materials such as cement-based composites require a special approach to the surface classification and a special application of roughness numbers. There is a large series of roughness numbers based on different definitions but in principle they all characterize surface irregularities, i.e. the height protrusions (peaks) and the depth depressions (valleys) of surfaces. Some of them are well correlated to such important quantities of cement-based materials as porosity, compressive strength or water-to-cement ratio [4–7]. This noteworthy property makes them attractive for further study.

The roughness parameters are computed either from two-dimensional (2D) profiles measured by contact/non-contact profilometers or from three-dimensional (3D) digital surface reliefs determined by a more advanced technique, e.g., laser scanning devices [8], including the laser scanning confocal microscopes [4–7,9,10].

By computing roughness numbers from digital 2D-profiles or 3D-surface reliefs a basic conceptual problem emerges whose solution inevitably influences the numerical values of roughness numbers and requires a special treatment if these numbers are to be properly used. The core of the problem consists in the fact that the values of roughness numbers strongly depend on the position and the analytical type of the so-called reference level that has to be introduced into the digital profile to compute those numbers. In addition, when the surface consists of a superposition of irregularities of various length-scales, the roughness numbers also show different values for different length-scales.

The goal of this paper is to tackle the mentioned obstacles and to find an acceptable way of solving the problems, especially in the case of fracture surfaces. Prior to the discussion of the studied problem in Sections 3 and 4, a short overview of the confocal surface reconstruction is presented in Section 2, while in Section 5 some applications to cement pastes illustrate and complement the topic. In concluding Section 6 the main results are summarized.

2. Confocal sections and digital surface reconstruction

Scanning confocal microscopes are optical microscopes with a very small depth of field which ensures that the confocal images show only those parts of objects that are very near to the focal

* Corresponding author. Tel.: +420 541 147 661.
E-mail address: ficker.t@fce.vutbr.cz (T. Ficker).

0008-8846/$ – see front matter © 2012 Elsevier Ltd. All rights reserved.
doi:10.1016/j.cemconres.2012.03.007

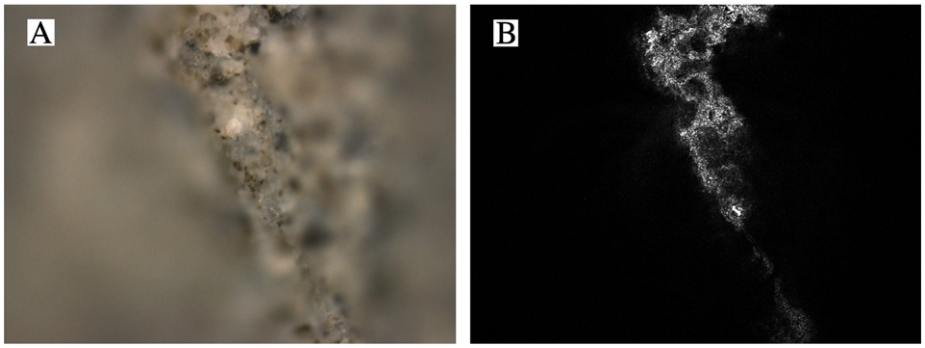

Fig. 1. Microscope images of fracture surfaces of cement paste: A) a non-confocal image with blurred margins; B) a confocal image with sharply visible points and removed blurred parts.

plane while other parts, farther from the focal plane, are invisible on the images. This is illustrated in Fig. 1. Part A of this figure shows non-confocal image with blurred left and right margins which represent points of the fracture surface that are out of the focal plane. In the central region of this image there are sharply imaged points localized in the focal plane. The points from the blurred regions are excluded from the confocal image Fig. 1B leaving only the sharp points from the central region. Fig. 1B is the so-called confocal optical section, which contains only sharply imaged points from the given position of the focal plane. Stepping the focal plane through a range of vertical positions provides a series of confocal optical sections from which the software reconstructs a 3D surface digital map (surface relief) illustrated in Fig. 2. The *z*-resolution, i.e. optical sectioning thickness, depends on a number of factors: the wavelength of the light used, pinhole size, numerical aperture of the objective lens, refractive index of components in the light path and the assembly of the instrument. The easiest and quickest estimation of convenient z-steps is to perform preliminary tests based on a series of probing optical *z*-sections. However, commercial confocal microscopes usually offer an automatic procedure for setting optimum input parameters.

Thanks to very shallow optical fields of confocal microscopes the final 3D surface reliefs contain only sharply imaged points of the fracture surface and their heights within the reliefs are determined from the positions of corresponding optical sections. As soon as the surface is digitally reconstructed, a discrete function f of the two variables x and y is available. It is the relief function $f(x, y)$ that analytically describes the fracture surface (Fig. 2).

3. Critical position of reference level in the digital surface relief

There are standard procedures for determining surface texture from measured profiles developed by machinery engineers and technologists [11,12]. In principle, these procedures comprise three main steps: fitting, filtering and analysis. Fitting raw data of a metallic surface means removing any unwanted geometry from the surface data such as global tilting or nominal curvature. This involves fitting the raw profile with a reference level in the form of a slanted straight line (i.e. first order polynomial) or arc (second order polynomial) or a polynomial of higher order. The fitting procedure results in the so-called primary profile, which is subjected to filtering. Filtering, as a second step in processing primary profiles, is usually based on passing a Gaussian, weighted average through the primary data to obtain the so-called waviness profile. The waviness profile is smoother than the primary profile. The stage of smoothing depends on the 'cutoff wavelength' used as a parameter within the Gaussian filter. The cutoff wavelength determines a border between the waviness and roughness profiles. The roughness profile comprises the slightest surface irregularities (peaks and valleys). It represents the finest scale of profile residues. Once all the profiles are separated, i.e. the primary, waviness and roughness profiles, the third step of the morphology

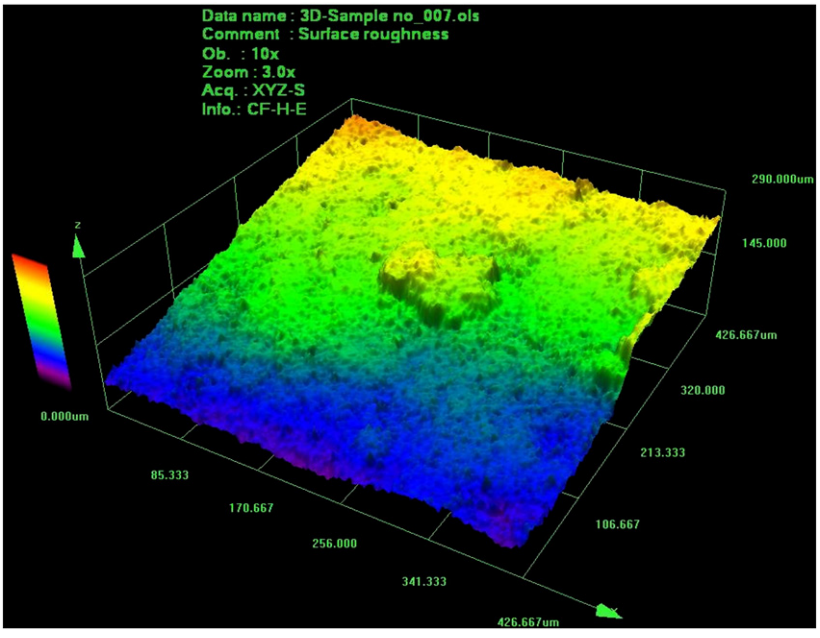

Fig. 2. Confocal reconstruction of fracture surface — digitally created 3D-profile.

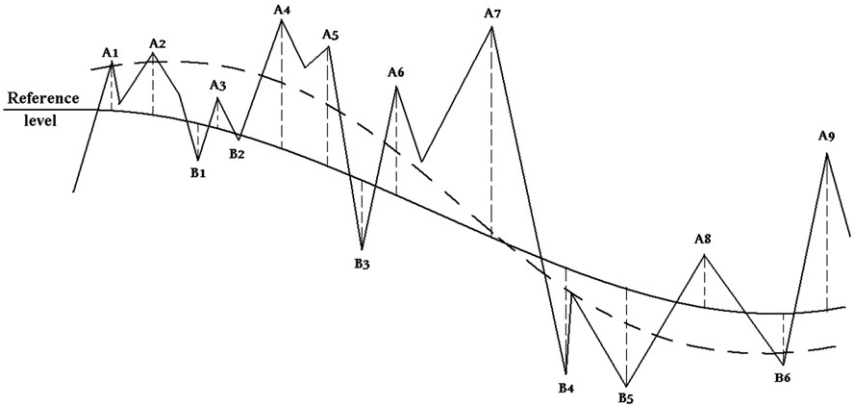

Fig. 3. A scheme of surface profile with marked central level.

analysis may start. The analysis of the irregularities within the roughness profile results in the so-called *R*-values, i.e. roughness numbers. Hundreds of different definitions of roughness number have been proposed, some of which are described in ISO standard 251787 [11]. The frequently used roughness parameters are the arithmetic average R_a and the root mean square (rms) R_q. It should be mentioned that the value of cutoff wavelength implemented within the Gaussian filter has a huge impact on the values of all the roughness numbers. Choosing a shorter cutoff wavelength will result in smaller roughness numbers. To prevent an arbitrary choice of the cutoff value and to encourage a consistent approach to this item, ISO standard 4288-1996 [12] presents a table of standard cutoff values along with selection recommendation.

The evaluation of surface irregularities described in the preceding paragraph concerned especially metallic surfaces that were processed to attain a required 'smoothness'. However, dealing with non-metallic materials and their fracture surfaces, whose profiles are not processed but are a result of natural fracture processes, requires an alternative approach. In the next paragraphs it will be shown that fitting and filtering procedures can be realized also within the Fourier analytical scheme in a quite natural way that respects the hierarchical structure of fracture surfaces. The Fourier fitting and filtering procedures are performed by using the partial Fourier sums with a variable number of terms. The number of terms in those sums has a similar meaning as the cutoff parameter within the Gaussian filter. A detailed description of this method is presented in Section 4.

As was mentioned in the introduction, numerical expressions of surface irregularities necessarily require positioning some reference level that ideally goes through the central parts of the digitalized profile, as is schematically indicated in Fig. 3. In the case of the 2D-profile it is the central curve and in the case of the 3D-profile it is the central 'surface', i.e. the central level. Unfortunately, there is no precise, general method for finding ideal positions for these central objects and, thus, in practice some type of fitting procedures has to be employed to reach a satisfactory result. Usually a polynomial is chosen as a fitting pattern for the central object but its order is set intuitively even though it has a considerable influence on the values of the resulting profile roughness numbers. The higher the order of the polynomial, the better it follows the contours of the digital profile and the smaller are the differences between the reference level and the profile and, as a consequence, lowering the roughness numbers appears. In such a case it is difficult to find an acceptable compromise.

Under these circumstances it should not be surprising that two independent computations of profile numbers may lead to different results due to the different polynomial orders. Treating such results without knowing properly under what conditions they were achieved results in a real risk of faulty conclusions and misinterpretation of otherwise reliable measurements. A comparison of two profile numbers which resulted from different processing conditions has no meaning. For all these reasons it is essential to specify properly the fitting pattern used and the type of fitting procedure.

4. Fourier scheme

To explore behavior of a more sophisticated central pattern, we implemented the Fourier series $F(x, y)$ as a functional object positioned in the 3D-profile $f(x, y)$

$$\begin{aligned} F(x,y) &= \lim_{N\to\infty} F_N(x,y) \\ &= \lim_{N\to\infty} \sum_{k,n=0}^{N-1} \lambda_{kn} \left(a_{kn} \cos\frac{k\pi x}{p} \cos\frac{n\pi y}{q} + b_{kn} \sin\frac{k\pi x}{p} \cos\frac{n\pi y}{q} + \right. \\ &\left. + c_{kn} \cos\frac{k\pi x}{p} \sin\frac{n\pi y}{q} + d_{kn} \sin\frac{k\pi x}{p} \sin\frac{n\pi y}{q} \right) \end{aligned} \tag{1}$$

where $2p$ and $2q$ specify the length and the width, respectively, of the investigated sample

$$\begin{aligned} &\Omega = \{x \in (-p,+p), y \in (-q,+q)\} \\ &a_{kn} = \frac{1}{pq} \iint_\Omega f(x,y) \cos\frac{k\pi x}{p} \cos\frac{n\pi y}{q} dxdy \\ &b_{kn} = \frac{1}{pq} \iint_\Omega f(x,y) \sin\frac{k\pi x}{p} \cos\frac{n\pi y}{q} dxdy \\ &c_{kn} = \frac{1}{pq} \iint_\Omega f(x,y) \cos\frac{k\pi x}{p} \sin\frac{n\pi y}{q} dxdy \\ &d_{kn} = \frac{1}{pq} \iint_\Omega f(x,y) \sin\frac{k\pi x}{p} \sin\frac{n\pi y}{q} dxdy \\ &\lambda_{kn} = \left\{ \begin{array}{ll} 1 & (k>0,\ n>0) \\ 1/2 & k=0,\ n>0 \quad or \quad k>0,\ n=0 \\ 1/4 & k=n=0 \end{array} \right\} \end{aligned} \tag{2}$$

At first sight it might seem that we do not perform any fitting procedure like e.g. the method of least squares but the integrations (Eq. (2)) included in the Fourier scheme in fact ensure such an optimization, which is analogous to the method of least squares. The main difference between the optimization of polynomials by the method of least squares and the Fourier integration method consists in the different bases they use. The method of least squares performed with polynomials employs a non-orthogonal basis, whereas Fourier integration is performed within the orthogonal basis of harmonic functions. An identical mathematical background of the least square method and the Fourier procedure is discussed and explained in Appendix A.

By increasing N in Eq. (1), we increase the number of terms (N^2) in the partial Fourier function $F_N(x, y)$,[1] which has the same effect as increasing the order of polynomials. Increasing the number of terms

[1] By 'term in the Fourier series' we understand the whole expression in the parentheses in Eq. (1).

makes the Fourier surface follow more closely the contours of the 3D-profiles and this decreases the values of roughness numbers because the absolute differences between the 3D-profile and the Fourier surface, i.e. $|f(x, y) - F(x, y)|$, become smaller. For this reason it is extremely important to specify clearly what number N has been chosen for the reference surface and this information must accompany the calculated profile numbers. Unfortunately, there is no exact quantitative measure determining the best value of N. This situation is analogous to that of the cutoff Gaussian wavelengths whose values were specified [12] on an empirical basis rather than from an exact theory. The choice of the particular reference level within the Fourier scheme will be discussed in the next section after the investigation of the capability of partial Fourier's functions (Eq. (1)) to converge on our measured 3D profiles.

Since the partial sums $F_N(x, y)$ of Fourier's series (Eq. (1)) do not always converge, it is necessary to investigate their convergence capability, i.e. to check the limiting behavior $\lim_{N\to\infty} F_N(x, y)$. This convergence behavior can be observed with the so-called delta function $\Delta(N)$, which may be expressed in the discrete form as follows:

$$\Delta(N) = \frac{1}{K \cdot L} \sum_{i=1}^{K} \sum_{j=1}^{L} \left[f\left(x_i, y_j\right) - F_N\left(x_i, y_j\right) \right] \tag{3}$$

where $K \cdot L$ is a pixel resolution of the used images. The delta function $\Delta(N)$ is a real function and may assume both the positive and negative values, i.e. $\Delta(N) \in (-\infty, +\infty)$. In case of convergence, i.e. $\lim_{N\to\infty} F_N(x, y) = f(x, y)$, the function $\Delta(N)$ will approach zero

$$\lim_{N\to\infty} \Delta(N) = 0 \tag{4}$$

This auxiliary criterion of convergence will be used in the next section as a testing tool investigating the convergence capability of partial Fourier's functions $F_N(x, y)$ within the present morphological study of the fracture surfaces of hydrated cement pastes.

Finally, to illustrate the behavior of profile numbers in practical applications, the following two profile/roughness numbers are introduced as probing tools:

$$H_a(N) = \frac{1}{K \cdot L} \sum_{i=1}^{K} \sum_{j=1}^{L} \left| f\left(x_i, y_j\right) - F_N\left(x_i, y_j\right) \right| \tag{5}$$

$$H_q(N) = \sqrt{\frac{1}{K \cdot L} \sum_{i=1}^{K} \sum_{j=1}^{L} \left[f\left(x_i, y_j\right) - F_N\left(x_i, y_j\right) \right]^2} \tag{6}$$

The roughness number H_a actually represents an average of absolute irregularities whereas H_q is a root mean square (rms) of those irregularities. Both these numbers are frequently used in surface roughness analyses of metallic materials and have been tested recently as indicators of mechanical quantities of hydrated cement materials [4–7]. They both show statistically reliable characteristics.

5. Applications to fracture surfaces of cement paste

As has been mentioned, we have recently studied morphology of the fracture surfaces of hydrated cement pastes by roughness numbers of different kinds [4–7] to investigate their correlation to porosity and other related volume quantities of cement-based materials. A confocal microscopy was employed in those studies to reconstruct 3D-profiles in the form of digital replicas. When computing roughness numbers from digital replicas, we encountered difficulties with an optimum position of reference surface and initiated an alternative procedure different from that used for industrially processed metallic surfaces. This procedure seems to be suitable for cementitious.

For illustrative purposes several specimens consisting of hydrated cement pastes were selected from a set of one-year old specimens. Ordinary Portland cement was used for their preparation. The specimens were mixed with the water-to-cement ratio equal to 0.4, and the fresh paste was cast in molds of a size $2 \times 2 \times 10$ cm^3. The paste was cured at a temperature of 20 ± 2 °C, and relative humidity of 100% for three months. Then, the specimens were fractured in the three-point bending arrangement and sectioned into small cubes $2 \times 2 \times 2$ cm^3. The rest of time the cubes were stored at normal laboratory conditions (20 ± 2 °C, ~101.325 kPa, 60 ± 10% RH). After 1 year some of those cubes were subjected to surface roughness analysis.

Fig. 4 shows the image of the 3D digital profile reconstructed from microscopic sections (magnification 20×, area of optical field 1 mm^2, pixel resolution 1024×1024). The Fourier series defined by Eq. (1) was implemented into the digitally reconstructed profile. The number of Fourier's terms was gradually increased starting from $N = 2$ (4 parenthesis terms) up to $N = 20$ or 50 (400 or 2500 parenthesis terms). The delta function $\Delta(N)$as an indicator of convergence was calculated according to Eq. (3) and can be seen in Fig. 5. Since the $\Delta(N)$approaches zero, in agreement with Eq. (4), a reliable convergence of the partial Fourier sums $F_N(x, y)$ may be anticipated.

The second step in our morphology analysis requires the selection of a reference level, i.e. a convenient number N that would specify a corresponding Fourier's function $F_N(x, y)$. There is no rule or convention for such a selection. This situation is analogous to that of metrology of metallic surfaces where the polynomials of the 'first' or higher orders are used. Since the machining metallic surfaces are rather plane, the polynomials of the first and second orders usually comply with their basic 'form geometry'. However, if the metallic surfaces were more wavy and rougher, or in the case of the fracture surfaces of cementitious materials or rocks, then a much higher order of polynomials would be necessary. It means that also within the Fourier's method a larger N-number should be anticipated in order to ensure a correct description of the 'basic geometry' of surfaces. The term 'basic geometry' reflects more or less the situation with metallic samples as they are usually nominally curved or tilted due to the machinery processing. However, fracture surfaces of cement-based materials result from the stochastic crack propagation and thus they often manifest unclear basic geometry that does not allow unambiguous placement of the reference surface (level). On the other hand, using a wider set of reference surfaces $F_N(x, y)$ with gradually increasing N, one can study the profile behavior by means of $H_a(N)$ and $H_q(N)$ on still finer length scales and in this way investigate the distribution of surface irregularities spanning over a broad band of texture and roughness formations.

For the sake of illustration, in the first row of Fig. 6 there are three images showing three different Fourier reference surfaces (levels) for $N = 2$, 7 and 20 (from the left to the right), which were derived from

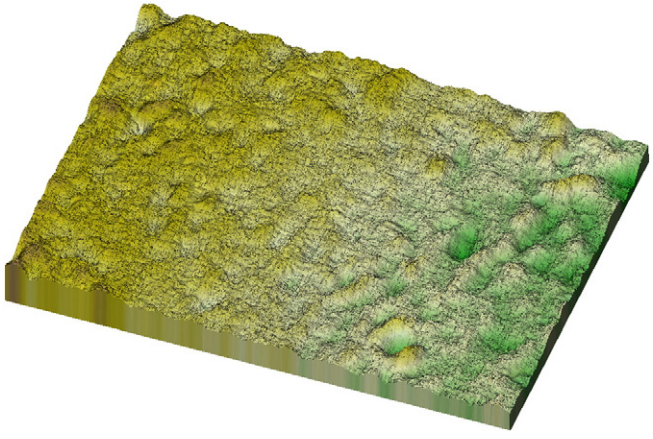

Fig. 4. 3D fracture surface of hydrated ordinary Portland cement paste.

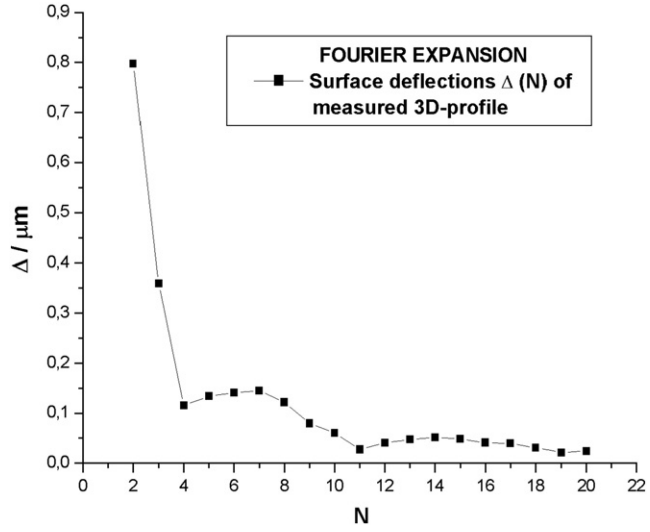

Fig. 5. The graph of delta function $\Delta(N)$ computed as differences between the 3D-profile and the Fourier reference level. The tendency $\lim_{N\to\infty}\Delta(N)\to 0$ confirms the right convergence behavior of the Fourier functions $F_N(x, y)$, which subsequently approach the measured 3D relief shown in Fig. 4.

the measured 3D-profile of the fracture relief displayed in Fig. 4. Comparing these three images it is obvious that for higher values of N the reference levels are wavier since they approach more closely the wavy shape of the real profile (Fig. 4). In the second row of Fig. 6 there are the same reference levels but augmented by the protrusions (marked in brown in the color images or by darker gray tones in the black-and-white images). The protrusions form roughness structures rising above the reference levels and when comparing these structures it can be seen that with higher N the roughness structures become finer and denser (a larger number of discrete peaks). In fact, the images in the second row of Fig. 6 do not show the complete peaks but only their sections with reference surface (see color islands). The third row of Fig. 6 also contains the reference levels for $N=2$, 7 and 20 but they are decorated by depressions (valleys) directed below the reference levels. The color of these depressions is blue in the color images or dark-gray in the black-and-white images. And again we can find finer and denser structures of those depressions when going from $N=2$ to $N=20$ (from the left to the right in the third row of Fig. 6).

From the structural changes presented in Fig. 6 it is possible to derive general conclusions concerning both protrusions and depressions, namely that at low values of N they both do not cover the reference areas too dense. Accordingly, the surfaces modeled with such low values of N are rather rough and thus yield large values of roughness numbers H_a and H_q (see Fig. 7). The largest values (7.5–11.5) μm of the functions in Fig. 7 can be observed at $N<5$ but then their values quickly decrease in the interval $N\in(5, 20)$ whereas for still larger values $N>20$ the decrease is only moderate.

Those structural and functional phenomena remind us of a great importance of selecting the reference level 'appropriately' because its position within the studied profile has a huge impact on roughness numbers $H_{a?}$ and $H_{q?}$. As already stated, there is no general rule for positioning the reference level; we can rely either on an intuitive way supported by empirical practice or adopt an 'artificial' rule, which would allow researchers to assume a unified approach to the selection procedure. For example, it would be possible to employ the delta function $\Delta(N)$ for this purpose. By normalizing the graph $|\Delta(N)|$ to unity, i.e. $|\Delta(1)|=1$ and fitting the graph with a smooth function $\Phi(N)>0$, we could find a number N_r of the reference level $F_{N_r}(x, y)$ by means of the equation $\Phi(N_r)=0.1$, whose right side represents one tenth of the initial value $\Phi(1)\approx 1$. Other rules are also possible but there is a question whether all those rules would be meaningful. It seems to us that a more reasonable concept would be to adopt the fact that the surface texture and the surface roughness are scale dependent properties of fracture surfaces and to treat them accordingly. A good alternative is to move the reference level $F_N(x, y)$ within the 3D profile by means of a sufficiently large interval of N-values and quantify those surface properties by using properly defined functions similar to those of $H_a(N)$ and $H_q(N)$. Introducing the reference levels with subsequently increasing N-values we actually change the length scale on which the surface texture/roughness is analyzed (the higher the N-value, the smaller the length scale). This means that on different length scales different texture/roughness

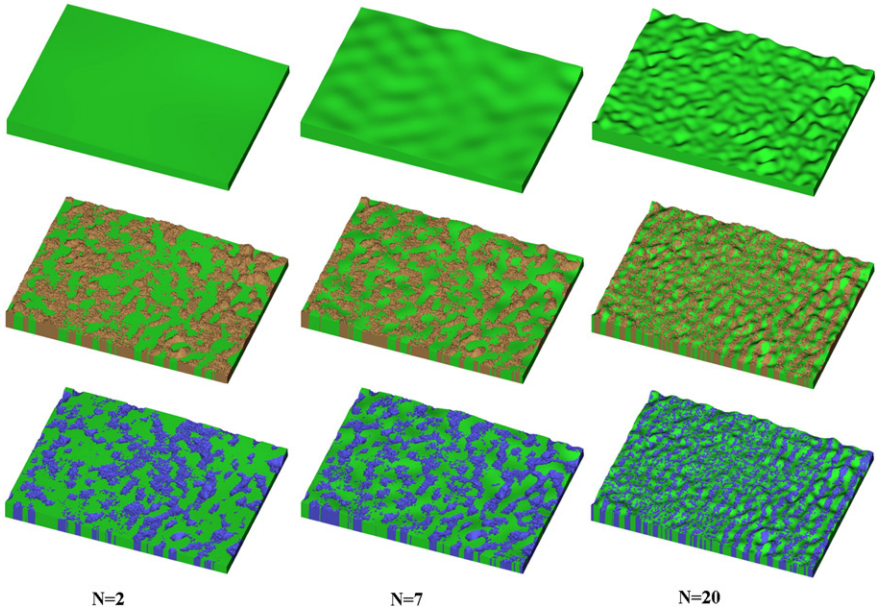

Fig. 6. Three different 3D Fourier's reference levels (green color) corresponding to $N=2$, 7 and 20 along with their modifications showing protrusions (brown color) and depressions (blue color). All the reference levels are derived from the measured 3D-profile presented in Fig. 4.

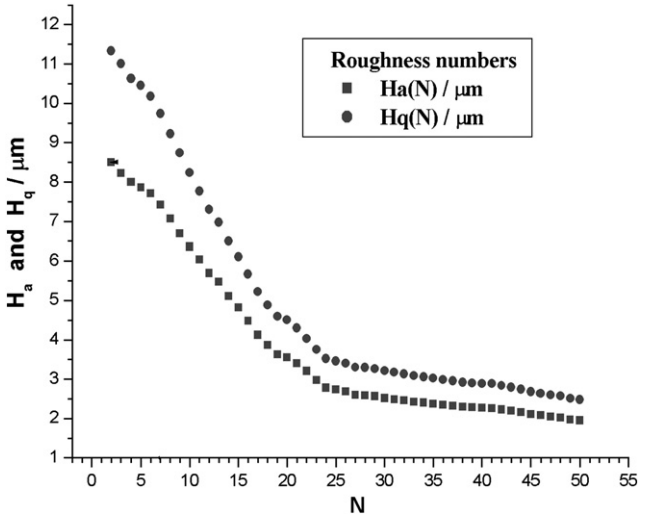

Fig. 7. The graphs of roughness numbers $H_a(N)$ and $H_q(N)$ illustrating their decreasing tendency caused by adding the terms in the Fourier series.

can be found and quantified. However, these quantities are valid only for a given scale and thus have only restricted (local) meaning. Looking for a global indicator of the 'overall' texture/roughness, one should analyze the surface functions like $H_a(N)$ and $H_q(N)$, and introduce a parameter or parameters characterizing their 'overall functional behavior'. To find such 'overall' indicators (if they exist) is not a straightforward matter and will require more research.

6. Conclusion

Finding an optimum reference levels within digital 3D surface profiles is a general problem that concerns all the calculation methods that could be used. The position as well as the shape of the reference level considerably influences the values of profile/roughness numbers computed from the 3D-profiles, and thus it would be important to specify conditions under which these values are determined.

The numerically processed data, which were originally measured on fracture surfaces of cement pastes, have indicated that fracture surfaces in contrast to industrially processed metallic materials have practically no 'basic geometry', and thus there is practically no aid for adequate positioning the reference level. In addition, the surface texture/roughness as a scale dependent property cannot be anchored to a single length-scale but requires analyzing all length scales present in the surface irregularities of the investigated samples. The multi-wave Fourier scheme proved to be a very convenient tool for this purpose. It allows quantifying the surface texture/roughness subsequently for different length scales by means of moving reference level and creating a broad spectrum of values of profile/roughness parameters. In this way an overview of the profile/roughness behavior in a wide range of length scales may be available and the corresponding quantitative output may be subjected to further analyses.

Acknowledgements

This work was supported by the Ministry of the Czech Republic under contract no. ME 09046 (Kontakt). Thanks are also due to Professor H. M. Jennings (Massachusetts Institute of Technology, USA) for his interest and support.

Appendix A. Equivalence between the method of least squares and Fourier's expansion

In this section we show that the method of least squares and the Fourier expansion method have the same mathematical background. First we formulate the general method of least squares and then on this basis we derive the Fourier expansion coefficients. For simplicity we discuss only one-dimensional case but the derivation in two dimensions would be analogous. The following derivation should not be considered as a rigorous mathematical proof but rather as a popular explanation which nevertheless contains a sound core. Such a popular explanation has been chosen to make it easier for the broadest class of readership.

Let us have a function $f(x)$ defined in the interval(α, β). It can be approximated by means of basis functions $\phi_o(x)$, $\phi_1(x)$, $\phi_2(x)$, ... $\phi_r(x)$ in the same interval as follows

$$f(x) = c_o\phi_o(x) + c_1\phi_1(x) + c_2\phi_2(x) + \ldots\ldots + c_p\phi_p(x) = \sum_{k=0}^{r} c_k\phi_k(x) \quad (7)$$

Let the function $f(x)$ be specified in a discrete form by a set of couples of points$\{f(x_i), x_i\}_{i=1}^{n}$. The expansion coefficients c_k may be optimized by the method of least squares to fit the set of the points (regression method). For this purpose a sum S of squares is introduced

$$S = \sum_{i=1}^{n}\left[f(x_i) - \sum_{k=0}^{r} c_k\phi_k(x_i)\right]^2 = \min \quad (8)$$

and its minimum is sought

$$\frac{\partial S}{\partial c_k} = 0, k = 0,\ 1,\ 2, \ldots\ldots r \quad (9)$$

which leads to a more straightforward algebraic expression

$$\frac{\partial S}{\partial c_k} = -2(a_k - c_1a_{k1} - c_2a_{k2} - \ldots\ldots - c_ra_{kr}) = 0 \quad (10)$$

where

$$a_k = \sum_{i=1}^{n} f(x_i)\phi_k(x_i), \quad a_{kh} = \sum_{i=1}^{n}\phi_k(x_i)\phi_h(x_i), \quad k,\ h = 0,\ 1,\ 2, \ldots\ldots ra \quad (11)$$

Eqs. (10) and (11) define a system of linear algebraic equations

$$\begin{aligned} &a_{00}c_0 + a_{01}c_1 + \ldots\ldots + a_{0r}c_r = a_0 \\ &a_{10}c_0 + a_{11}c_1 + \ldots\ldots + a_{1r}c_r = a_1 \\ &\ldots\ldots\ldots\ldots\ldots\ldots\ldots\ldots \\ &a_{r0}c_0 + a_{r1}c_1 + \ldots\ldots + a_{rr}c_r = a_r \end{aligned} \quad (12)$$

whose solution provides optimized expansion coefficients $\{c_k\}_{k=0}^{r}$ related to Eq. (7). This scheme is applicable with any arbitrary groups of basis functions $\phi_k(x)$. For example, if the polynomial regression of third order is to be performed, then the basis functions are defined as follows: $\phi_1(x) = 1$, $\phi_2(x) = x$, $\phi_3(x) = x^2$, $\phi_4(x) = x^3$ and Eq. (7) assumes the form of the polynomial of third order

$$f(x) = c_o + c_1x + c_2x^2 + c_2x^3 \quad (13)$$

The polynomial basis represents a non-orthogonal basis, since the off-diagonal terms a_{kh} of Eqs. (12) are non-zero, i.e. $a_{kh} = \sum_{i=1}^{n}\phi_k(x_i)\phi_h(x_i) \neq 0$, and as a consequence the full system of linear algebraic equations (12) has to be solved.

On the other hand, with an orthogonal basis the off-diagonal terms in system (12) are identically zero, i.e. $a_{kh} = \sum_{i=1}^{n}\phi_k(x_i)\phi_h(x_i) = 0$, and

system (12) is considerably simplified. In this case the expansion coefficients c_k may be computed straightforwardly as follows

$$c_k = \frac{a_k}{a_{kk}} = \frac{\sum_{i=1}^{n} f(x_i)\phi_k(x_i)}{\sum_{i=1}^{n} \phi_k(x_i)\phi_k(x_i)} \tag{14}$$

Now let us apply the procedure of least squares to Fourier's scheme. The Fourier set of trigonometric functions $\{1,\ \cos\frac{\pi x}{b},\ \sin\frac{\pi x}{b},\ \cos\frac{2\pi x}{b},\ \sin\frac{2\pi x}{b},\ \ldots\ldots\ \cos\frac{r\pi x}{b},\ \sin\frac{r\pi x}{b}(r\to\infty)\}$ represents an infinite orthogonal basis defined within a continuous interval $(-b,\ +b)$ so that the algebraic system (12) now contains an infinite number of equations and the members of that system should be investigated within the continuous representation. The transition from discrete to continuous representations can 'schematically' be realized by shortening the equidistant length Δx between points x_i to an infinitesimally small value, i.e. $\Delta x \to 0$. The off-diagonal elements then assume integral forms

$$a_{kh} = \lim_{\Delta x\to 0} \sum_{i=1}^{n} \phi_k(x_i)\phi_h(x_i)\Delta x = \int_{-b}^{+b} \phi_k(x)\phi_h(x)dx = \\ = \left\{ \begin{array}{l} \int_{-b}^{+b} \sin\left(\frac{k\pi x}{b}\right)\cos\left(\frac{h\pi x}{b}\right)dx = 0 \\ \int_{-b}^{+b} \sin\left(\frac{k\pi x}{b}\right)\sin\left(\frac{h\pi x}{b}\right)dx = 0 \\ \int_{-b}^{+b} \cos\left(\frac{k\pi x}{b}\right)\cos\left(\frac{h\pi x}{b}\right)dx = 0 \end{array} \right\} \quad \text{for } k \neq h \tag{15}$$

Provided $f(x)$ is a periodic function in the interval $(-b,\ +b)$ with the period $2b$, we can find the Fourier expansion coefficients by means of Eq. (14) as follows

A) For $k > 0$

$$c_k = \lim_{\Delta x\to 0} \frac{\sum_{i=1}^{n} f(x_i)\phi_k(x_i)\Delta x}{\sum_{i=1}^{n} \phi_k(x_i)\phi_k(x_i)\Delta x} = \frac{\int_{-b}^{+b} f(x)\phi_k(x)dx}{\int_{-b}^{+b} [\phi_k(x)]^2 dx} \\ = \frac{\int_{-b}^{+b} f(x)\phi_k(x)dx}{b} = \\ = \left\{ \begin{array}{l} \frac{1}{b}\int_{-b}^{+b} f(x)\cos\left(\frac{k\pi x}{b}\right)dx = c_k^{(c)} \\ \frac{1}{b}\int_{-b}^{+b} f(x)\sin\left(\frac{k\pi x}{b}\right)dx = c_k^{(s)} \end{array} \right\} \tag{16}$$

B) For $k = 0$

$$c_0 = \frac{1}{2b}\int_{-b}^{+b} f(x)dx = c_0^{(c)} = c_0^{(s)} \tag{17}$$

Inserting the expansion coefficients $c_k^{(c)}$ and $c_k^{(s)}$ from Eqs. (16) and (17) into Eq. (7), the usual Fourier series emerges

$$f(x) = \sum_{k=0}^{\infty} \left[c_k^{(c)} \cos\left(\frac{k\pi x}{b}\right) + c_k^{(s)} \sin\left(\frac{k\pi x}{b}\right) \right] \tag{18}$$

The foregoing derivation has confirmed that Eq. (18) can be viewed as a result of the optimizing procedure of least squares, in which an infinite and continuous basis of periodic trigonometric functions has been employed.

References

[1] K. Ravi-Chandar, W.G. Knauss, An experimental investigation into dynamic fracture: II microstructural aspects, Int. J. Fract. 26 (1984) 65–80.
[2] D. Dalmas, C. Guera, J. Scheibert, D. Bonany, Morphological aspects and deterministic reconstruction of dynamical fracture surfaces in brittle materials, EPJ Web Conf. 6 (2010), doi:10.1051/epjconf/20100639010 39010-p1–3910-p2.
[3] J. Scheibert, C. Guera, F. Célarié, D. Dalmas, D. Bonamy, Brittle–quasibrittle transition in dynamic fracture, Phys. Rev. Lett. 104 (2010) 045501-1–045501-4.
[4] T. Ficker, D. Martišek, H.M. Jennings, Roughness of fracture surfaces and compressive strength of hydrated cement pastes, Cem. Concr. Res. 40 (2010) 947–955.
[5] T. Ficker, D. Martišek, H.M. Jennings, Surface roughness and porosity of hydrated cement pastes, Acta Polytech. 51 (2011) 7–20.
[6] T. Ficker, Fracture surfaces and compressive strength of hydrated cement pastes, Constr. Build. Mater. 27 (1) (2012) 197–205.
[7] T. Ficker, D. Martišek, Roughness and fractality of fracture surfaces as indicators of mechanical quantities of porous solids, Cent. Eur. J. Phys. 9 (2011) 1440–1445, doi:10.2478/s11534-011-0061-0.0.
[8] K.-R. Wu, A. Yan, J. Liu, D. Zhang, W. Yao, Reconstruction and analysis of 3-D profile of fracture surface of concrete, Cem. Concr. Res. 30 (2000) 981–987.
[9] D.A. Lange, H.M. Jennings, S.P. Shah, Analysis of surface-roughness using confocal microscopy, J. Mater. Sci. 28 (14) (1993) 3879–3884.
[10] D.A. Lange, H.M. Jennings, S.P. Shah, Relationship between fracture surface roughness and fracture behavior of cement paste and mortar, J. Am. Ceram. Soc. 76 (3) (1993) 589–597.
[11] ISO 25178-2, Geometrical product specifications (GPS)—surface texture: areal—part 2: terms, definition and surface texture parameters (International Organization for Standardization, Geneva, 2012).
[12] ISO 4288-1996, Geometrical product specification (GPS)—surface texture: profile method—rules and procedures for the assessment of surface texture, (International Organization for Standardization, Geneva, 1996).